CHAPTER II

BASALTS

2.1 Introduction

The Nguu and Ngulai Hills volcanic subterranes are built up with several small volcanic cones and vents lying next to each other forming a cluster of the cones and giving off basaltic lavas covering the areas. Remnants of these volcanic cones are obvious on a satellite image (Figure 1.2). Geographically, both the study sub-areas are distinctively separated volcanic fields belonging to the Northern Chyulu Hills Volcanic lavas as defined by Späth *et al.* (2000). According to the geologic map created by Saggerson (1963), the Nguu basalts are equivalent to Plb1 analcime basanite unit, whereas the Ngulai basalts are equivalent to Plb2 olivine basalt unit overlying the Sutan Hamud-Emali-Simba lavas (Plb1) (Figure 1.3).

Massive basaltic lava flow outcrops in the Nguu hills areas can be observed in several spots, particularly along the creek channels running out from the cone center. Therefore, most of the samples from this area were collected from outcrops. On the contrary, a good exposure of basaltic flow in the Ngulai area could not be observed because this area is covered by red soil and volcanic debris; even on the cone flanks, they are covered up by loose ash and lapilli. Consequently, all the basalt samples from the Ngulai area were picked from either lapilli layers or floats. For comparative purpose, a few fresh olivine basalt samples of the recent Chyulu lavas exposed in the vicinity of Kiboko town nearby the study area were also collected. Hereafter, the samples of the Chyulu lavas will be referred as "Kiboko basalts."

2.2 Petrographic Description

There are 18 basalt specimens selected for petrographic investigation. Among them, 7 specimens (*KNg01, 02, 03, 09, 10, 11 and 12*) were sampled within the same basaltic field around Nguu hills. Eight specimens from the Ngulai basaltic field were taken from 4 different cones, including Kwa Nthuku (*KKNt02, 03 and 04*), Kyanduini (*KKyd01, 02 and 04*), Kwa Mbiti (*KKMb02*), and Ol Doinyo Orkaria (*KOk01*). The other samples were collected from 3 different spots within the Chyulu basaltic lavas exposed east of Simba in the vicinity of Kiboko, including *KKb01* from

a rock quarry located just north of Omaki cone (~7 km SEE of Simba), *KKb02* from a lava flow cropped out near the Hunter's Lodge (~16 km SE of Simba) and *KKb03* from Mwailo cone near the Kiboko Agricultural Research Institute (~4.5 km S of the Hunter's Lodge) Petrographic description and field information of these basalts are reported below.

2.2.1 Nguu Hills Basalts

This basaltic field, mapped as a part of "analcime basanites (Plb1)" unit by Saggerson (1963), is located north of the Muoni river. It consists of at least 3 basalt layers intercalated with pyroclastic beds, erupted from the volcanic vent of Nguu and its satellites, to form a composite cone of Nguu. The cone flanks have been partly eroded away. These basalts bear xenoliths of several rock types, e.g. mafic granulites, felsic granulites, garnet-bearing granitoids, hornblende-biotite gneisses, peridotites and pyroxenites. The felsic granulite, granitoid and gneiss may be of the underlying basements. The mafic granulite, which is predominant but unlikely akin to any basement formations exposed in the vicinity, are presumably derived from a deep-seated source underneath. More detail on the xenoliths will be reported in Charpter III.

Macroscopically, the basalt specimens are generally dense and have a flinty-looked with bluish black color. The rocks are slightly vesicular, 5-10% vesicles, and moderately porphyritic, up to 10% phenocrysts. The phenocrysts are mainly olivine (up to 2 mm in size) setting in fine-grained groundmass. Some olivine phenocrysts are completely altered to yellow-brown iddingsite.

Under a polarizing microscope, the rocks display microporphyritic texture in aphanitic to fine-grained matrix of plagioclase, augite, olivine and magnetite (Figure 2.1). The majority of phenocrysts are olivine. Most phenocrysts are sub-idiomorphic to allotriomorphic grains. The olivines, both phenocrysts and a matrix constituent, are replaced by bright brownish orange iddingsite and black spots of magnetite in various stages. In some specimens, the matrix is almost entirely replaced by iddingsite, e.g. *KNg09* (Figure 2.1c). Embayments and rounded outlines are common features of most large grains that are mostly xenocrysts. Composite xenocrysts (such as olivine-spinel) can be observed (Figure 2.1d). Plagioclases as a matrix constituent are in a form of microlites, locally displaying faint alignment, interstitial with pale brown idiomorphic grains of augite and titanomagnetite. Plagioclase and

rare clinopyroxene xenocrysts are observed (Figure 2.1e). Large clinopyroxene xenocrysts always have reaction rinds (Figure 2.2f).
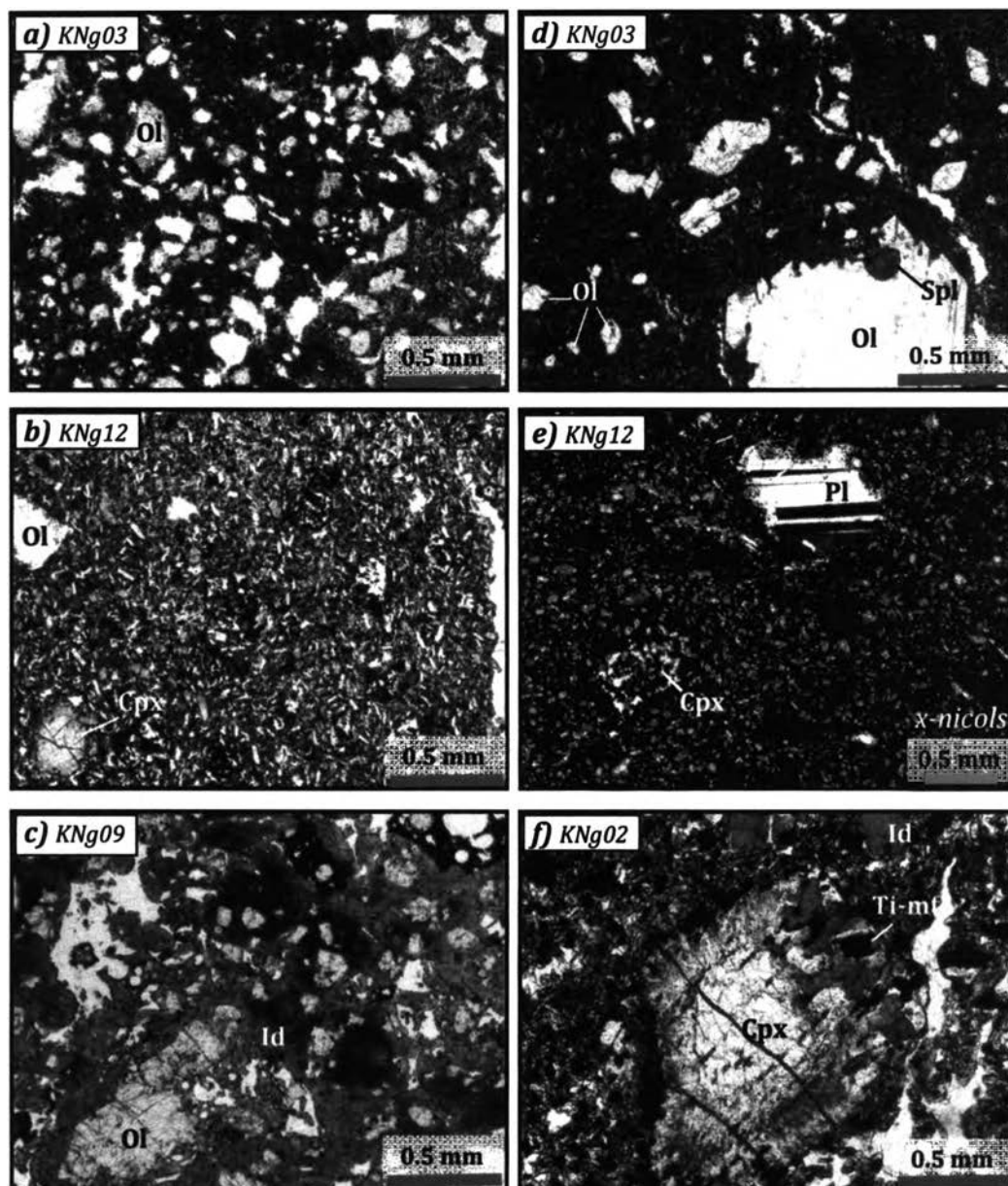

Figure 2.1 Photomicrographs of basalt samples from the Nguu Hills area showing microporphyritic textures with various sizes of phenocrysts, xenocrysts and groundmass, stages of iddingsite (Id) replacement and vesicle contents. (*a*) Finest matrix with low Id substitution. (*b*) Coarser matrix with moderate Id substitution. (c) Most part of matrix replaced by Id. (*d*) Size differences among olivine (Ol) phenocrysts and a spinel (Spl)-Ol composite megacryst (e) Plagioclase (Pl) and clinopyroxene (Cpx) xenocrysts. (*f*) Rare Cpx xenocryst with symplectic rind and abundant titanomagnetite (Ti-mt) in groundmass.

2.2.2 Ngulai Hills Basalts

This basaltic field was mapped as a part of "olivine basalts (Plb2)" unit in which the lavas had been given off from a cluster of small volcanic cones of Ngulai Hills (Saggerson, 1963). These basalts also bear several xenolith types similar to the Nguu basalts with additional types of amphibolites and plagioclase-rich granulites. The peridotites are, however, rarely observed, while the pyroxenites are much more abundant.

Generally, the Ngulai basalt specimens share the same appearance with the Nguu basalts. Macroscopic differentiation between them is barely plausible, except some specimens from Kwa Nthuku which bear abundant pyroxene megacrysts. This feature is not observed in samples from the Nguu basalts. In addition, most of Ngulai basals are seldom experienced iddingsite replacement, except those from Ol Doinyo Orkaria. The vesicular basalt from Ol Doinyo Orkaria is very resembling to the Nguu basalts.

Microscopically, the rocks display a microporphyritic texture in aphanitic to fine-grained seriate matrix of plagioclase, augite, olivine and magnetite (Figure 2.2). The Ngulai basalts are relatively richer in microphenocryst content, up to about 30% by mode in some specimens. The majority of phenocrysts are olivine and clinopyroxene. Plagioclase phenocrysts are sparingly observed. Most phenocrysts are sub-idiomorphic to idiomorphic grains. Quartz xenocrysts rimmed by thin reaction rinds (Figure 2.2b) are common in some specimens, particularly those from Kyanduini cone. Xenolithic fragments of pyroxenite are normally observed as well. Composite xenocrysts such as titanomagnetite-clinopyroxene and clinopyroxene-spinel (Figure 2.2e) are more common than the Nguu basalts.

2.2.3 Chyulu Basalts

The Chyulu basalts, which have been accumulated by magmas from a number of vents located further south of the Nguu Hills area. These vents are distributed along a system of NW-SE and N-S trending weak zones and was mapped as "olivine basalts (Rvb)" unit (Saggerson, 1963). In this study, a small fraction of the Chyulu basalts were investigated only around the vicinity of Kiboko and few samples were collected for a comparative purpose. Every part of the Chyulu basalts where observed does not enclose any deep-seated xenoliths. Since the studied samples do
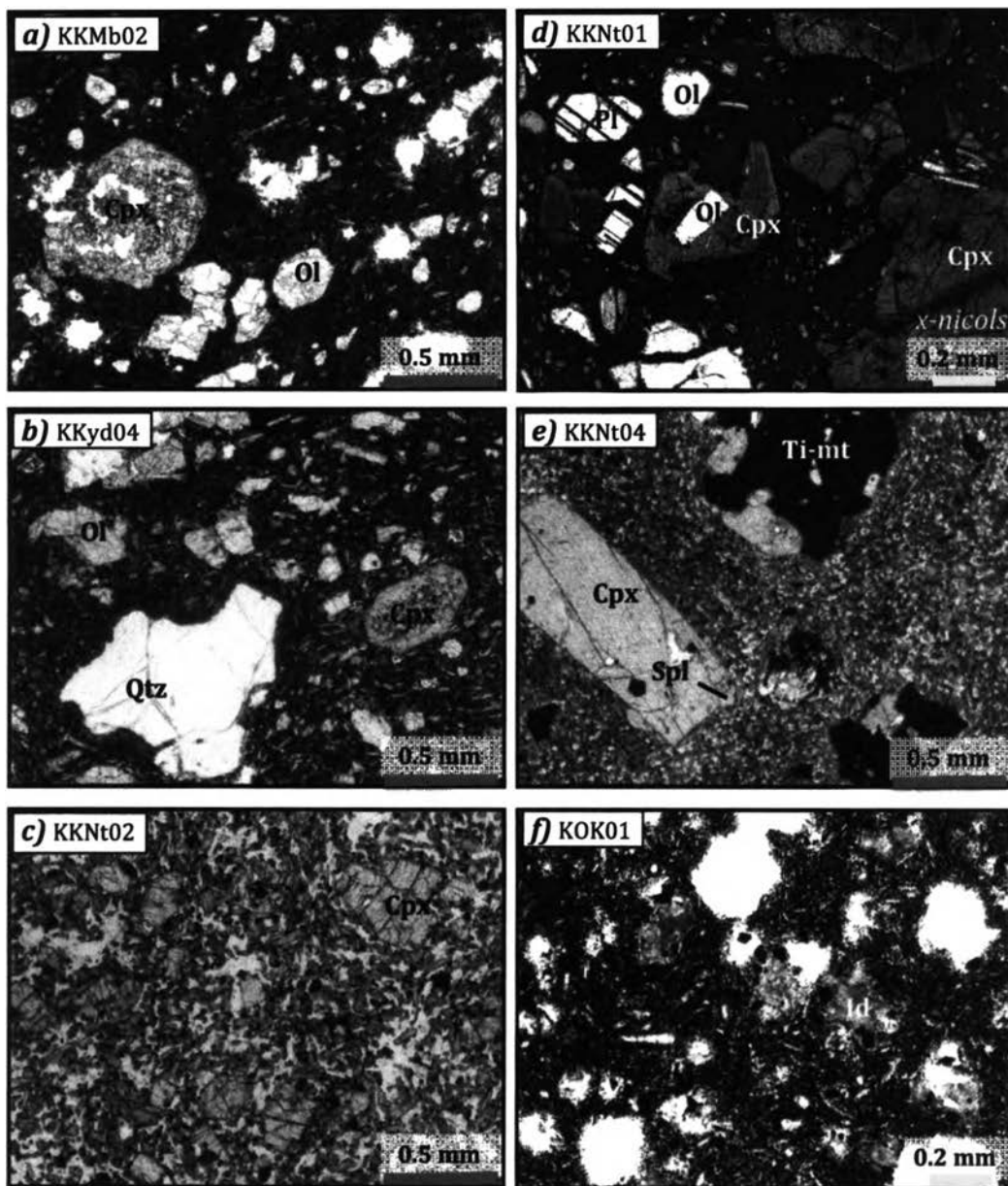
Figure 2.2 Photomicrographs of basalt samples from the Ngulai Hills area showing microporphyritic textures with various sizes of phenocrysts, xenocrysts and groundmass, and vesicle contents. *a*) Sub-idiomorphic olivine (Ol) and clinopyroxene (Cpx) phenocrysts in finest matrix from Kwa Mbiti. *b*) Quartz (Qtz) xenocryst with Ol and cpx phenocrysts in coarser microlite matrix from Kyanduini. c) Cpx microphenocrysts in fine seriate matrix from Kwa Nthuku. *d*) Sub-idomorphic Cpx, Ol and plagioclase (Pl) phenocrysts in finest matrix from Kwa Nthuku resemble to that from Kwa Mbiti. *e*) Titanomagnetite (Ti-mt) and spinel (Spl) composited with Cpx xenocrysts from Kwa Nthuku. *f*) Basalt with moderate iddingsite (Id) replacement from Ol Doinyo Orkaria.
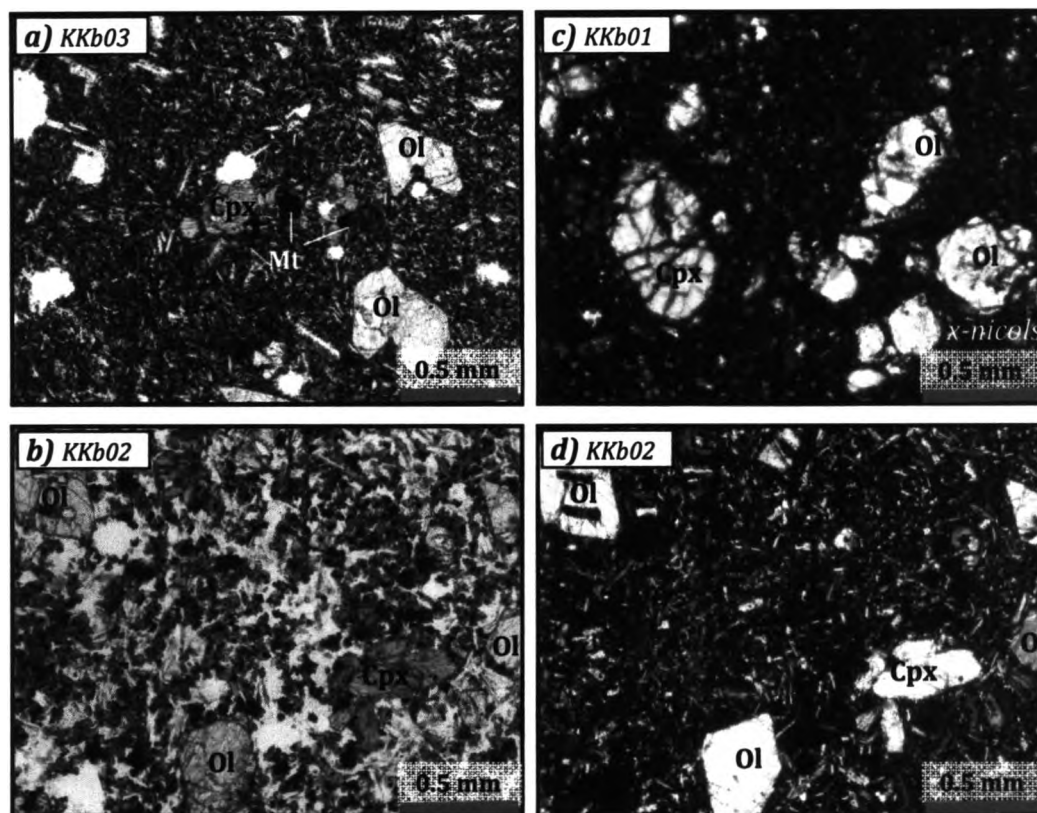
Figure 2.3 Photomicrographs of basalts from the Chyulu basalts showing microporphyritic textures containing common olivine (Ol) and clinopyroxene (Cpx) and some magnetite (Mt) phenocrysts in fine-grained groundmass. *a*) Sub-idiomorphic phenocrysts with partial alignment of microlite matrix from Mwailo cone. *b*) Cpx glomerocrysts in magnetite and coarser microlite matrix forming randomly interlocking texture from basaltic flow near Hunter's Lodge, Kiboko. *c*) Compositional zoning in cpx phenocryst, from basaltic flow near Omaki cone, faintly displayed. *d*) Black holes of fine vesicles interlocked among microlite matrix clearly observed.

not represents the whole Chyulu basalt unit, here after these basalt samples will be referred as "Kiboko (Chyulu) basalts".

The collected specimens are microporphyritic, and relatively fresher than the Nguu and Ngulai basalts specimens. Microscopically, they contain about 5 to 8% microphenocrysts. The phenocrysts are chiefly olivine and clinopyroxene, with relatively uniform size (about 0.3-0.5 mm) sitting in fine-grained microlites. The microlites in the finer-matrix specimen display partial alignment (Figure 2.3a), whereas those in the coarser matrix are more randomly oriented interlocking texture (Figure 2.3b). Most phenocrysts are sub-idiomorphic. Larger clinopyroxene

phenocrysts are commonly zoned (Figure 2.3c). Clinopyroxene glomerocrysts are often observed (Figure 2.3b).

2.3   Geochemical Characteristics

Twenty two basalt specimens from all the three areas were selected for whole-rock geochemical analyses. All analytical techniques were reported in Chapter I. Among these selected samples, nineteen of them are from corundum (ruby)-related basaltic patches (10 from the Nguu field and 9 from the Ngulai field). The rest are from other basaltic patches exposed around Kiboko, which are a part of the Chyulu lavas and presumably are corundum-barren type. All the analyses on major oxides, CIPW norm and selected trace elements of each specimen are presented in Tables 2.1-2.4 and the ranges of major oxides and selected trace elements are summarized in Table 2.5.

2.3.1 Rock Discrimination

Based on LeBas *et al.* (1986) classification scheme, most specimens in this study fall within foidite region with slightly extending into picrobasalt and tephrite/basanite" fields (Figure 2.4a). Comparatively, on Cox *et al.* (1979) scheme, some specimens are in the fields of basanite/tephrite and picrite; however, there are several others fall out off the classification fields (Figure 2.4b). All the basalts investigated are in alkaline series (Figure 2.4b-c). In addition, all the samples sit within the oceanic Island basalts (OIB) or rift field according to the Th-Zr/117-Nb/18 tectono diagram (Wood, 1980).

Basaltic lavas from the Nguu Hills area were geochemically classified as "basanite and olivine basalt" by Saggerson (1963) and as "picrobasalt / basanite" by Spåth *et al.* (2000). In this study, these rocks chemically belong to foidite-tephrite/basanite suite based on LeBas *et al.* (1986) classification scheme. For Cox *et al.* (1979) diagram, most the specimens fall off the fields due to silica under-saturated in nature while the rest are in the fields of basanite/tephrite and picrite. Two briefly parallel fractionation trends are displayed. The first trend is relatively higher total alkaline contents and composed of samples *KNg02, KNg03, KNg08a and KNg05a*, which are arranged in an approximate manner of increasing fractionation degree. This trend will be referred as *"Nguu I"* trend. The other trend consists of

samples *KNg09, KNg11, KNg01, KNg10, KNg06a and KNg12,* and will be referred as *"Nguu II"* trend. According to the CIPW norm calculation, all the Nguu samples are olive-normative basaltic rocks approximately containing olivine 10-20, hypersthene 0-14, nepheline 0-6.35 wt % and ilmanite 6-12 wt % norm. Mg# ranges from ~64 to 86 and An contents from ~41 to 75. At equivalent SiO_2 contents, samples from the *Nguu I* trend seem to have higher ilmanite normative contents but lower Mg# than those from the *Nguu II* trend.

For the Ngulai basaltic lavas, they were named as "olivine basalt" by Saggerson (1963) and as "basanite/alkali basalt/nephelinite" by Späth *et al.* (2000). In this study, they are plotted in the fields of foidite and tephrite/basanite of LeBas *et al.* (1986) diagram, with a wider distribution range than those from the Nguu Hills area. For Cox *et al.* (1979) classification diagram, the specimens also exhibit similar behavior as those from the Nguu Hills by either in the field of picrite extending into basanite/tephrite or off the fields due to silica under-saturated in nature. The majority of these samples seem to be ploted along those differentiation trends exhibited by the Nguu Hills samples. The first set following the *Nguu I* trend includes samples *KKNt01a, KKMb02, KKMb01a* and *KOK01.* The second set following the *Nguu II* consists of samples *KKNt03, KKYd03, KKYd02* and *KKNt02.* However, sample KKNt04, with the highest total alkaline content of about 5.2 wt % and nepheline normative (13 wt %), is displaced above the *Nguu I* trends in the field of tephrite/ basanite. On the basis of the CIPW norm, all the Ngulai Hills samples display olive-normative. The main normative contents are olivine 4 to 24, nepheline 0-13 wt % and ilmanite 6-9 wt % norm. Most of the Ngulai samples do not have hypersthene normative, except one sample, *KNt03,* comprising ~5 wt % norm. Mg# ranges from ~65 to 76 and An contents from ~38 to 85. Similar to the Nguu Hills samples, the samples following the *Nguu I* trend seem to have higher ilmanite normative contents, at equivalent SiO_2 contents, than those following the *Nguu II* trend.

For the Chyulu field, the basaltic lavas were named as "olivine basalt" by Saggerson (1963) and as "basanite/alkali basalt/hawaiite" by Späth *et al.* (2000). However, all the three specimens from the Kiboko area fall within the field of tephrite/basanite according to LeBas *et al.* (1986) and in basalt field, very close to the boundary between basalt and basanite, according to Cox *et al.* (1979). All the samples follow the *Nguu I* trend and represent the most differentiated part. Based on the

Table 2.1 Whole-rock analyses of major oxides and CIPW norm of basaltic lavas from the Nguu Hills area.

| | Nguu Hills | | | | | | | | | |
| | Nguu I trend | | | | Nguu II trend | | | | | |
Wt %	KNg 02	KNg 03	KNg 08a*	KNg 05a*	KNg 09	KNg 11	KNg 01	KNg 10	KNg 06a*	KNg 12a*
SiO_2	39.43	40.03	40.10	40.80	38.67	39.62	39.77	40.73	41.20	42.25
TiO_2	5.21	5.37	5.98	6.26	4.92	4.75	4.89	5.03	6.15	3.36
Al_2O_3	8.41	8.79	8.74	9.06	9.53	9.34	8.73	8.30	9.20	9.03
[1]Fe_2O_3	7.64	9.19	16.70	17.00	10.18	7.47	10.43	4.52	17.10	14.15
[2]FeO	7.32	5.83	n/a	n/a	5.16	7.34	4.52	10.72	n/a	n/a
MnO	0.18	0.18	0.19	0.19	0.19	0.19	0.19	0.18	0.19	0.19
MgO	13.27	14.44	12.40	10.70	14.73	15.59	16.12	15.83	11.40	12.98
CaO	11.20	10.10	10.40	10.70	10.00	9.86	9.57	9.32	10.30	11.34
Na_2O	2.42	2.01	2.64	2.45	0.76	1.23	1.36	2.01	1.45	2.29
K_2O	0.58	1.23	0.76	0.98	0.65	0.70	1.01	0.77	1.48	0.92
P_2O_5	0.66	0.68	0.73	0.58	0.78	0.62	0.62	0.62	0.49	0.94
H_2O^+	2.34	0.78	0.75	0.84	3.08	1.96	1.89	0.98	1.74	2.12
H_2O^-	0.34	0.21	n/a	n/a	0.63	0.35	0.25	0.33	n/a	0.29
Total	99.00	98.84	99.39	99.56	99.28	99.02	99.35	99.34	100.70	99.86
Wt %	CIPW normative mineralogy (%)[3]									
Orthoclase	3.79	7.63	4.85	6.15	3.84	5.15	5.97	5.06	9.04	5.44
Albite	9.95	7.54	10.62	12.09	6.43	10.41	11.51	14.76	11.86	11.65
Anorthite	10.19	11.15	9.57	10.65	20.67	17.39	14.73	11.10	14.08	11.64
Nepheline	5.70	5.13	6.35	4.68	0.00	0.00	0.00	1.22	0.22	4.18
Diopside	32.15	27.39	29.74	30.87	18.56	21.74	22.33	24.39	27.03	30.63
Hypersthene	0.00	0.00	0.00	0.00	13.80	2.87	1.07	0.00	0.00	0.00
Olivine	12.72	18.87	16.29	12.65	10.01	18.29	20.13	19.71	15.65	18.29
Ilmenite	9.89	10.20	11.36	11.89	9.34	9.02	9.29	9.55	11.68	6.38
Magnetite	10.19	8.45	7.05	7.25	2.99	10.64	1.02	0.70	7.08	6.06
Hematite	0.29	0.00	0.00	0.00	8.12	0.00	9.73	10.23	0.00	0.00
Apatite	1.53	1.58	1.69	1.34	1.81	1.44	1.44	1.44	1.14	2.18
Zircon	0.07	0.09	0.10	0.09	0.00	0.07	0.00	0.07	0.09	0.00
Chromite	0.13	0.12	0.09	0.09	0.00	0.12	0.00	0.15	0.10	0.00
[4]AN	49.11	58.21	45.93	45.36	75.18	61.16	54.68	41.47	52.80	48.50
[5]Mg#	75.59	73.69	67.49	63.87	83.58	78.81	86.41	86.19	64.90	72.06

a* represents a sample with Fe_2O_3 in a form of total Fe_2O_3

n/a = not analyzed; n.d. = not detected; n.d.** = not determined due to a weight-gaining effect caused by an oxidation of Fe^{2+} to Fe^{3+}.

[1]Fe_2O_3 is derived by subtraction of Fe_2O_3[(total)] from XRF method with FeO from wet chemical method.

[2]FeO is obtained from a titration technique.

[3]Calculated using software IgPet2007 and FeO values, when they are not available via chemical analyses, were estimated following Irvine and Baraka (1971).

[4]AN is an An content in plagioclase calculated using atomic proportion = Ca/ (Ca+2Na).

[5]Mg# is calculated using atomic proportion = Mg/(Mg+Fe^{2+}) where Fe^{2+} is from FeO content.

Table 2.2   Whole-rock analyses of major oxides and CIPW norm of basaltic lavas from the Ngulai Hills and Kiboko (Chyulu) areas.

| | Ngulai Hills | | | | | | | | | Kiboko | | |
| | Nguu I trend | | | | Nguu II trend | | | | | Nguu I trend | | |
wt %	KKMb 02	KKMb 01a*	KKNt 01a*	KOK 01	KKNt 02	KKNt 03	KKYd 02	KKYd 03	KKNt 04	KKb 01	KKb 02	KKb 03
SiO_2	39.53	43.80	38.20	44.25	44.78	40.70	43.07	42.84	41.78	42.75	43.53	44.44
TiO_2	4.03	3.90	4.94	3.94	3.12	3.74	3.34	3.40	3.87	3.14	3.65	3.33
Al_2O_3	8.59	12.40	7.66	12.90	10.40	9.66	9.14	9.28	11.27	11.86	12.60	13.64
Fe_2O_3	5.80	15.30	17.10	10.48	5.46	7.44	3.78	4.04	9.00	4.38	3.90	4.73
FeO	8.67	n/a	n/a	4.22	8.51	7.16	9.46	9.31	4.79	8.34	9.98	8.68
MnO	0.21	0.20	0.22	0.19	0.18	0.21	0.19	0.19	0.23	0.19	0.19	0.19
MgO	14.18	9.43	13.10	5.88	11.36	11.74	14.82	14.45	7.60	12.09	9.41	8.69
CaO	12.38	9.86	12.50	9.67	10.97	12.12	10.35	10.48	12.43	11.18	10.00	9.76
Na_2O	2.39	3.17	1.88	2.89	2.45	1.27	2.07	2.03	3.24	3.11	3.22	3.32
K_2O	0.88	1.44	0.72	1.98	1.04	0.88	1.16	1.12	2.03	1.22	1.45	1.36
P_2O_5	1.11	0.58	1.01	1.14	0.43	1.14	0.88	0.90	0.73	0.54	0.69	0.64
H_2O^+.	0.78	n.d.	1.74	1.25	n.d.	2.80	0.30	0.48	2.07	n.d.	n.d.	n.d.
H_2O^-	0.32	n/a	n/a	0.60	0.21	0.19	0.24	0.29	0.28	0.14	0.13	0.11
Total	98.87	99.36	99.07	99.39	98.87	99.05	98.80	98.81	99.32	98.94	98.07	98.89
wt %	CIPW normative mineralogy (%)[3]											
Or	5.71	8.87	4.69	12.35	6.51	5.71	7.22	7.05	13.30	7.57	8.93	8.40
Ab	1.59	15.23	0.80	24.39	16.53	10.75	10.99	11.25	3.46	5.94	12.93	17.66
An	9.86	15.17	10.12	16.05	14.13	17.80	12.04	12.68	9.56	14.62	15.46	18.12
Ne	10.10	6.28	8.18	0.04	2.28	0.00	3.53	3.21	12.98	11.04	7.75	5.65
Di	35.29	24.11	36.58	19.41	29.97	27.40	26.98	26.88	37.16	29.87	24.07	21.12
Hy	0.00	0.00	0.00	0.00	0.00	4.98	0.00	0.00	0.00	0.00	0.00	0.00
Ol	16.73	13.35	17.51	3.96	14.55	8.96	23.73	22.67	1.19	16.28	15.34	13.23
Il	7.65	7.41	9.38	7.48	5.93	7.10	6.34	6.46	7.35	5.96	6.93	6.32
Mt	8.41	7.35	6.60	2.83	7.92	10.79	5.48	5.86	4.94	6.35	5.65	6.86
Hem	0.00	0.00	0.00	8.53	0.00	0.00	0.00	0.00	5.59	0.00	0.00	0.00
Ap	2.57	1.34	2.34	2.64	1.00	2.64	2.04	2.09	1.69	1.25	1.60	1.48
Zr	0.07	0.07	0.10	0.12	0.03	0.10	0.07	0.07	0.06	0.06	0.07	0.07
Chr	0.12	0.07	0.07	0.03	0.10	0.09	0.15	0.15	0.06	0.12	0.07	0.06
[4]AN	85.42	48.42	92.23	38.29	44.61	60.96	50.80	51.52	72.27	69.89	52.98	49.16
[5]Mg#	74.46	64.63	67.41	71.30	70.41	74.51	73.63	73.45	73.88	72.10	62.70	64.09

a* represents a sample with Fe_2O_3 in a form of total Fe_2O_3

n/a = not analyzed; n.d. = not detected; n.d.** = not determined due to a weight-gaining effect caused by an oxidation of Fe^{2+} to Fe^{3+}.

[1]Fe_2O_3 is derived by subtraction of $Fe_2O_3^{(total)}$ from XRF method with FeO from wet chemical method.

[2]FeO is obtained from a titration technique.

[3]Calculated using software IgPet2007 and FeO values, when they are not available via chemical analyses, were estimated following Irvine and Baraka (1971).

[4]AN is an An content in plagioclase calculated using atomic proportion = Ca/ (Ca+2Na).

[5]Mg# is calculated using atomic proportion = Mg/(Mg+Fe^{2+}), where Fe^{2+} is from FeO content.

Table 2.3 **Whole-rock analyses of selected trace elements of basaltic lavas from the Nguu Hills area.**

ppm	Nguu Hills									
	Nguu I trend				Nguu II trend					
	KNg 02	KNg 03	KNg 08a*	KNg 05a*	KNg 09	KNg 11	KNg 01	KNg 10	KNg 06a*	KNg 12
Cs	0.5	0.4	0.4	0.4	n/a	0.2	n/a	0.6	0.3	n/a
Rb	23	28	301	43	n/a	14	n/a	18	34	n/a
Ba	482	433	446	471	n/a	1250	n/a	622	371	n/a
Th	6.3	6.5	7.3	6.7	n/a	5.9	n/a	6.1	6.5	n/a
U	1.5	1.6	2.0	1.5	n/a	1.0	n/a	1.7	1.8	n/a
Nb	84	88	96	96	n/a	80	n/a	81	92	n/a
Sr	780	975	747	718	n/a	1350	n/a	766	608	n/a
Hf	10	10	11	11	n/a	10	n/a	10	11	n/a
Zr	400	413	493	476	n/a	361	n/a	385	478	n/a
La	59	61	69	61	n/a	57	n/a	57	538	n/a
Ce	125	128	147	124	n/a	121	n/a	122	109	n/a
Pr	15	16	18	16	n/a	14	n/a	14	14	n/a
Nd	63	64	72	64	n/a	60	n/a	59	55	n/a
Sm	12	12	14	12	n/a	11	n/a	11	11	n/a
Eu	3.4	3.7	4.4	4.0	n/a	3.3	n/a	3.5	3.5	n/a
Gd	9.8	10.5	13.3	12	n/a	10.2	n/a	9.7	11	n/a
Tb	1.3	1.4	1.7	1.6	n/a	1.3	n/a	1.3	1.4	n/a
Dy	7.1	7.2	8.0	7.9	n/a	7.0	n/a	6.8	6.9	n/a
Ho	1.1	1.2	1.3	1.3	n/a	1.2	n/a	1.1	1.2	n/a
Er	2.5	2.9	3.4	3.4	n/a	3.2	n/a	2.8	3.1	n/a
Tm	0.3	0.3	0.4	0.4	n/a	0.3	n/a	0.3	0.4	n/a
Yb	1.9	2.0	2.2	2.2	n/a	2.1	n/a	1.8	2.3	n/a
Lu	0.3	0.3	0.3	0.4	n/a	0.3	n/a	0.3	0.3	n/a
Y	30	31	33	33	n/a	31	n/a	28	31	n/a
Pb	n.d.	n.d.	6	20	n/a	n.d.	n/a	n.d.	7	n/a
Sc	21	21	22	23	n/a	23	n/a	21	23	n/a
V	323	316	316	351	n/a	308	n/a	294	319	n/a
Cr	600	550	430	430	n/a	540	n/a	660	510	n/a
Ni	538	494	365	309	n/a	573	n/a	686	323	n/a
Ga	21	21	23	24	n/a	19	n/a	18	23	n/a

n/a = not analyzed; n.d. = not detected

Table 2.4   Whole-rock analyses of selected trace elements of basaltic lavas from the Ngulai
Hills and Kiboko (Chyulu) areas.

ppm	Ngulai Hills									Kiboko		
	Nguu I trend				Nguu II trend					Nguu I trend		
	KKMb 02	KKMb0 1a*	KKNt 01a*	KOK 01	KKNt 02	KKNt 03	KKYd 02	KKYd 03	KKNt 04	KKb 01	KKb 02	KKb 03
Cs	0.4	0.3	0.8	0.6	0.3	0.4	0.3	0.5	0.6	0.5	0.4	0.4
Rb	22	35	25	43	28	19	25	24	40	32	34	32
Ba	586	439	544	779	437	595	490	518	1650	447	446	466
Th	12	7	15	13	6	12	9	9	8	7	8	7
U	3.0	1.8	2.4	3.6	1.3	2.8	2.2	2.2	1.7	1.7	1.7	1.7
Nb	98	84	130	121	59	117	79	81	86	78	84	80
Sr	1300	747	1580	1470	675	5030	1050	1070	1230	728	814	815
Hf	9	8	11	14	5	12	8	8	8	7	9	9
Zr	396	367	527	577	158	503	346	357	307	281	342	346
La	107	58.4	121	118	61	119	82.6	84.9	67.2	56.9	65.4	61.3
Ce	223	121	254	229	104	234	164	170	130	113	135	124
Pr	26	14	30	28	12	28	19	20	15	13	16	14
Nd	104	57	120	108	48.5	109	77	81	62	53	64	60
Sm	19	11	22	20	9	20	14	15	11	10	12	10
Eu	5.6	3.4	6.8	5.9	2.8	5.7	4.4	4.5	3.3	3.2	3.4	3.4
Gd	16	10	20	15	8	15	12	12	10	9	10	9
Tb	2.1	1.3	2.5	2.0	1.2	2.1	1.6	1.7	1.3	1.2	1.4	1.2
Dy	11	7	12	10	7	10	8	8	7	6	7	7
Ho	1.7	1.1	1.9	1.6	1.2	1.7	1.3	1.4	1.2	1.1	1.2	1.3
Er	4.1	3.1	4.9	3.7	2.9	4.1	3.3	3.4	2.9	2.6	3.2	3.2
Tm	0.4	0.4	0.5	0.5	0.3	0.5	0.4	0.4	0.3	0.3	0.4	0.4
Yb	2.7	2.2	3.0	2.6	2.0	2.7	2.2	2.3	2.2	2.0	2.4	2.4
Lu	0.3	0.3	0.5	0.4	0.3	0.5	0.3	0.4	0.3	0.3	0.3	0.3
Y	42	29	49	44	30	42	34	36	30	28	31	31
Pb	5	8	15	11	n.d.	9	6	6	9	n.d.	n.d.	n.d.
Sc	24	22	23	19	22	22	22	22	23	24	21	20
V	300	279	302	324	285	281	267	271	331	283	272	249
Cr	520	350	360	150	450	440	700	680	240	570	350	280
Ni	366	201	323	161	317	296	483	463	107	315	192	182
Ga	21	23	22	27	20	23	19	19	20	20	22	22

n.d. = not detected

Table 2.5   Ranges of major and selected trace elements of the studied basalt samples.

	Nguu		Ngulai		Kiboko (Chyulu)	
	Max	Min	Max	Min	Max	Min
(Wt. %)						
SiO$_2$	42.25	38.67	44.78	38.20	44.44	42.75
TiO$_2$	6.26	3.36	4.94	3.12	3.65	3.14
Al$_2$O$_3$	9.53	8.30	12.90	7.66	13.64	11.86
Fe$_2$O$_3$(t)	17.10	14.15	17.10	14.29	14.99	13.64
MnO	0.19	0.18	0.23	0.18	0.19	0.19
MgO	16.12	10.70	14.82	5.88	12.09	8.69
CaO	11.34	9.32	12.50	9.67	11.18	9.76
Na$_2$O	2.64	0.76	3.24	1.27	3.32	3.11
K$_2$O	1.48	0.58	2.03	0.72	1.45	1.22
P$_2$O$_5$	0.94	0.49	1.14	0.43	0.69	0.54
AN	*75.18*	*41.47*	*92.23*	*38.29*	*69.89*	*49.16*
Mg#	*86.41*	*63.87*	*74.51*	*64.63*	*72.10*	*62.70*
(ppm)						
Cr	660	430	700	150	570	280
Ni	686	309	483	107	315	182
Rb	43	14	43	19	34	32
Ga	24	18	27	19	22	20

CIPW norm, the Kiboko lavas have olivine normative (13-16 wt %) without hypersthene normative. They also contain nepheline normative (6 to 11 wt %) and ilmanite normative (6-7 wt %). Mg# ranges from ~63 to 72 and An contents from ~49 to 70.

In general, all the basalts investigated are in alkaline series. The Nguu and the Ngulai basalts contain similar range of total alkali content. These rocks chemically belong to foidite-tephrite/basanite suite. Fractional crystallization seems to be the main process responsible for the compositional changing from foidite to basanite, as indicated by the positive slope of the observed total alkali trend against SiO$_2$ (Wilson, 1989). The Kiboko (Chyulu) specimens, on the other hand, fit nicely within the most fractionated area of the Nguu and Ngulai basalts. Two briefly parallel fractionation trends are displayed. The *Nguu I* trend is relatively higher in total alkaline and ilmanite normative contents. It is comprises of samples *KKNt01a, KNg02, KKMb02, KNg03, KNg08a, KNg05a, KKb01, KKb02, KKMb01a, KOK01* and *KKb03*. The *Nguu II* trend is composed of samples *KNg09, KNg11, KNg01, KKNt03, KNg10, KNg06a, KNg12, KKYd03, KKYd02* and *KKNt02*.
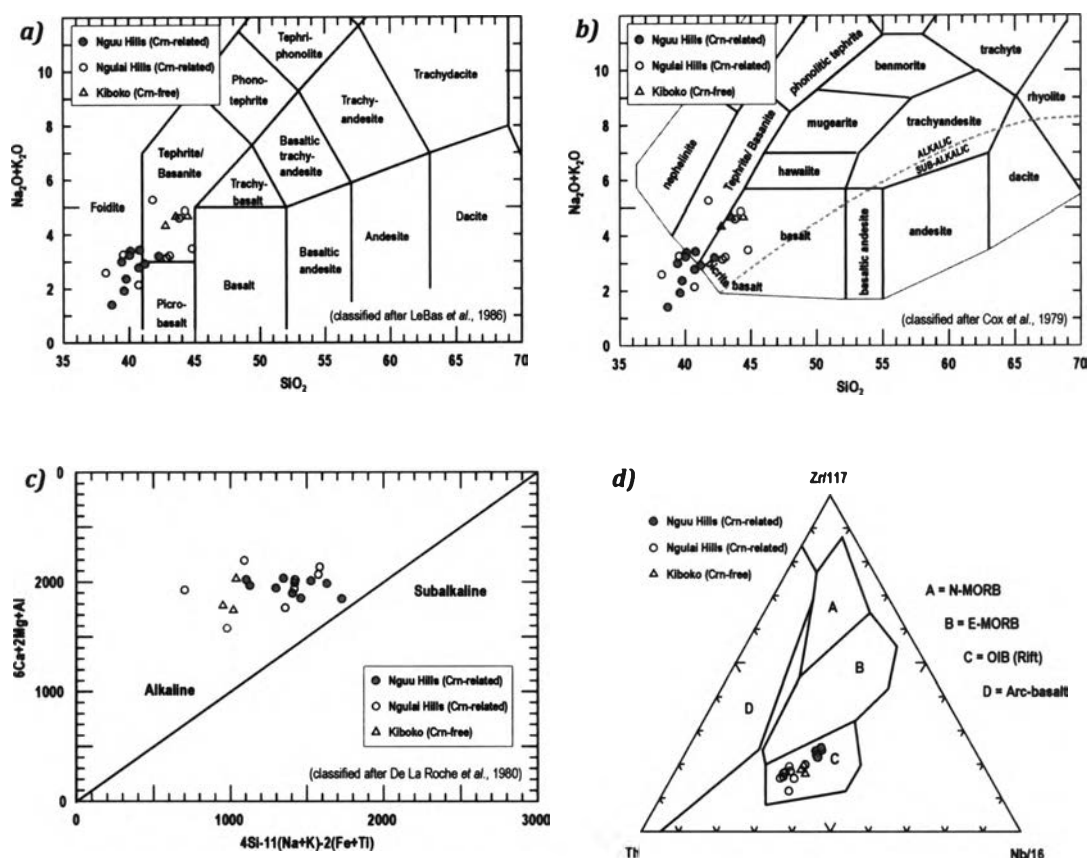
Figure 2.4. Classification diagrams for basalt samples of the study sites, which are Nguu, Ngulai, and Kiboko, a small part of the Chyulu lavas, basaltic fields. The dashed line dividing between alkaline and sub-alkaline lava series in (*b*) is after Miyashiro (1978). The Zr/117-Th-Nb/18 tectonomagmatic discrimination diagram (*d*) is after Wood (1980).

2.3.2 Whole-Rock Geochemistry

Based on the bivariant plots of major oxides against MgO (Figure 2.5), the Nguu lavas represent whole-rock compositions which approach to more mafic side, while Kiboko (Chyulu) basalts collected from Kiboko vicinity are more towards felsic affinity. The Ngulai basalts, on the other hand, have a widest range of SiO_2 values (38.2-44.8 wt %) covering those of the Nguu (38.7-42.3 wt %) and the Chyulu (42.7-44.4 wt %) on the more felsic end. This overlapping behavior also holds for some other major oxides, e.g. Al_2O_3, Na_2O and K_2O, as well as trace elements, e.g. Cr, Ni, Rb and Ga (Figures 2.5 and 2.6).

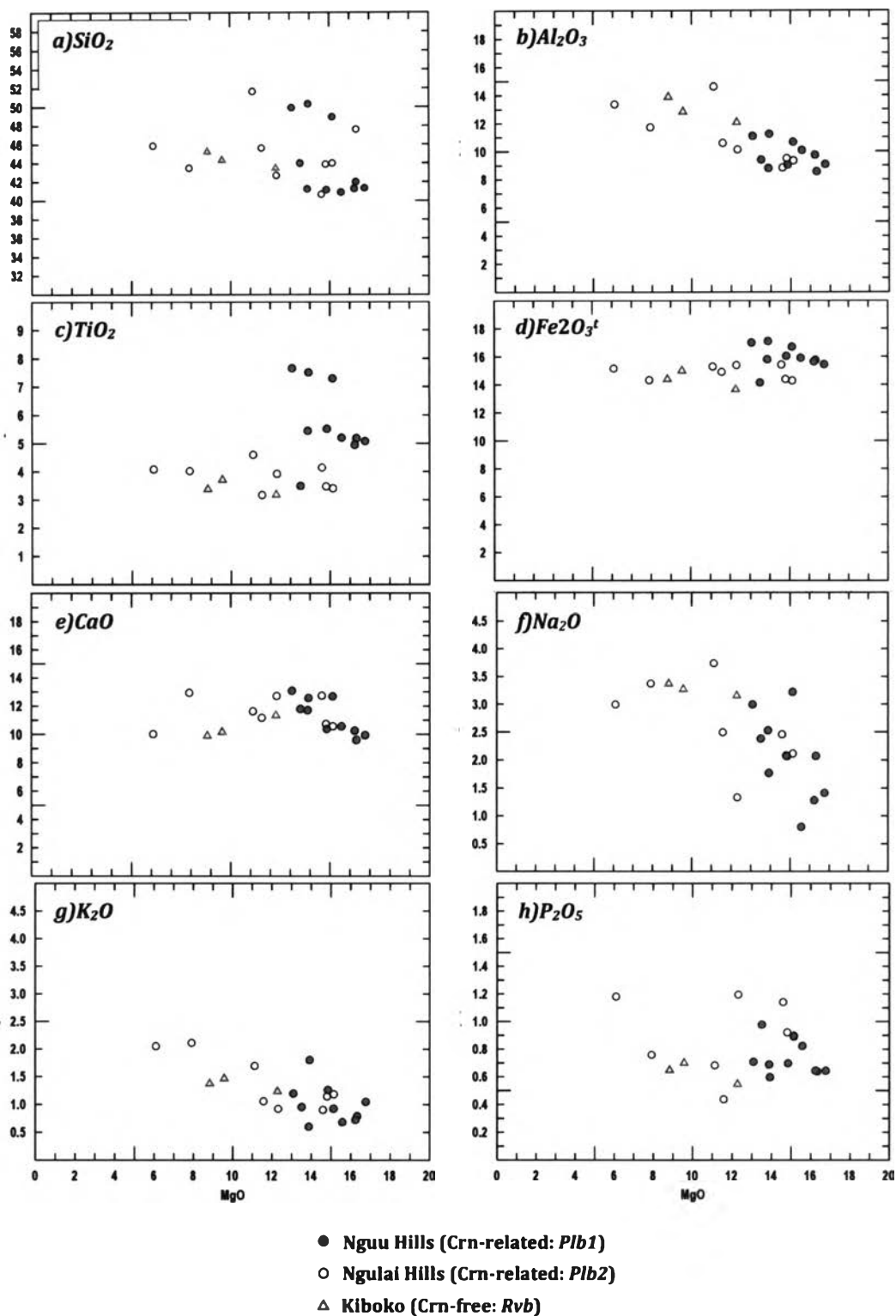Generally, these basalt specimens provide overall observable trends on

Figure 2.5 Plots of wt % major oxides versus wt % MgO for the basaltic rocks from the Nguu Hills, Ngulai Hills, and Kiboko (Chyulu) lavas. All oxides were normalized to 100 % on a volatile-free basis before plotting.
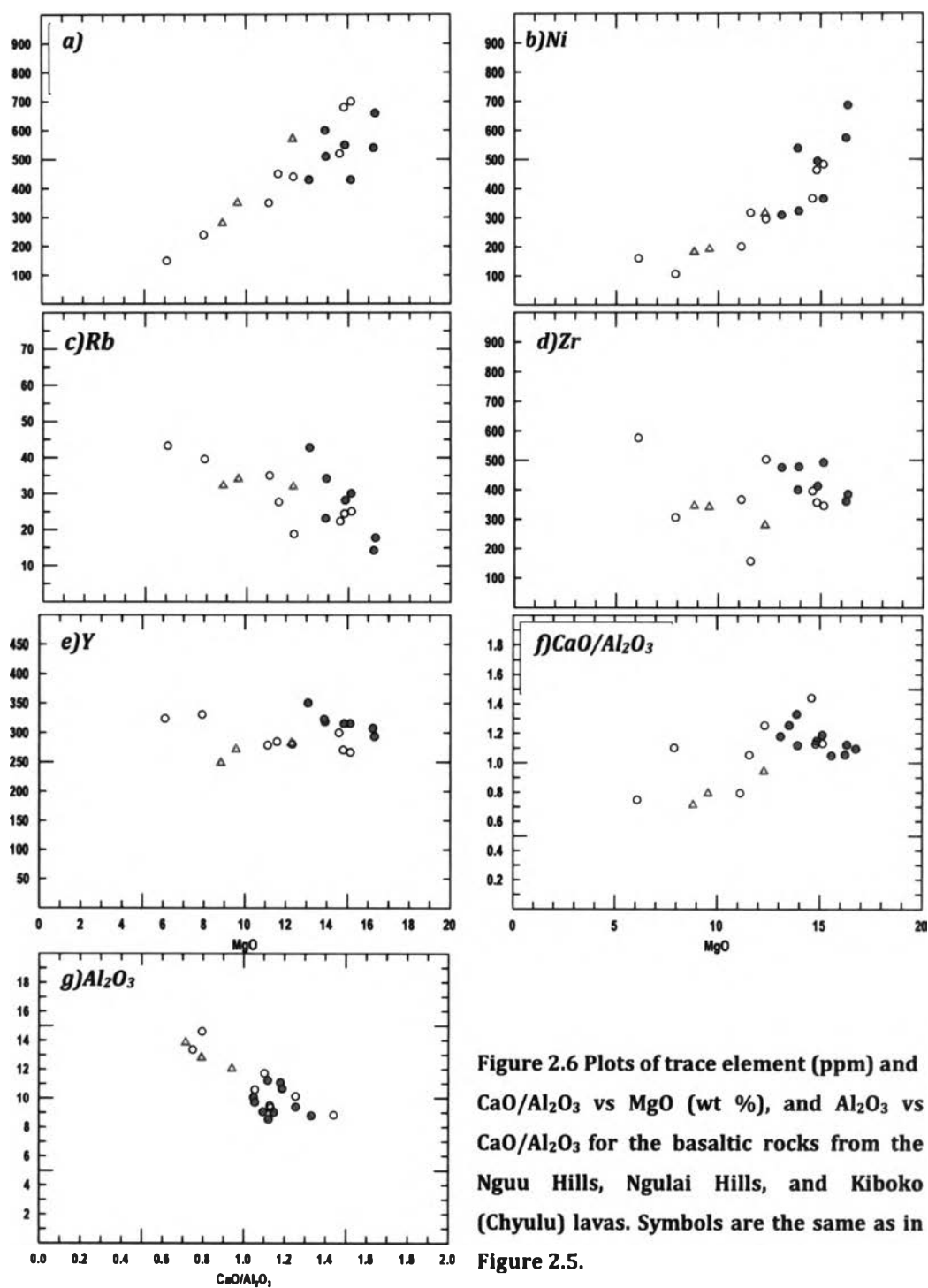
Figure 2.6 Plots of trace element (ppm) and CaO/Al_2O_3 vs MgO (wt %), and Al_2O_3 vs CaO/Al_2O_3 for the basaltic rocks from the Nguu Hills, Ngulai Hills, and Kiboko (Chyulu) lavas. Symbols are the same as in Figure 2.5.

correlation on plots of Al_2O_3, Na_2O, K_2O and Rb versus MgO (Figures 2.5b, f and g, and 2.6c), and less defined negative trends on SiO_2 and TiO_2 (Figures 2.5a and c). In addition, the whole suite exhibits nice positive correlation with MgO on some trace element plots including Cr and Ni (Figures 2.6a-b). These overall correlations

suggest a crystal fractionation process dominated by mafic phases. In correlation with petrographic data, olivine should be the most dominant phase to have crystallized during the earliest phase whereas lesser extent of clinopyroxene fractionation may also have taken place. Plagioclase, nevertheless, plays no significant role at this point.

Focusing into each individual volcanic field, some detailed characteristics of each field can be notable. Nguu Hills lavas can clearly be separated from those of the Ngulai Hills and the Kiboko (Chyulu) by their elevated TiO_2 and $Fe_2O_3^t$ values at similar MgO values (Figures 2.5c and d). The plots of SiO_2, TiO_2, CaO, $Fe_2O_3^t$ and Zr against MgO seem to further suggest that the Nguu basalts are likely composed of two subsets, *one (I)*, KKMb01, KNg05a, 06a, 8a, KKNt01a, with higher and *the other (II)* with lower SiO_2, TiO_2, CaO, $Fe_2O_3^t$ and Zr contents (Figures 2.5a, c, d and e, and 2.6f). The separation between these subsets can be repeatedly monitored on the plots of Ce, La, Rb versus Zr (Figures 2.7). On the contrary, the Ngulai and the Kiboko (Chyulu) basalts seem to be indistinguishable by these plots.
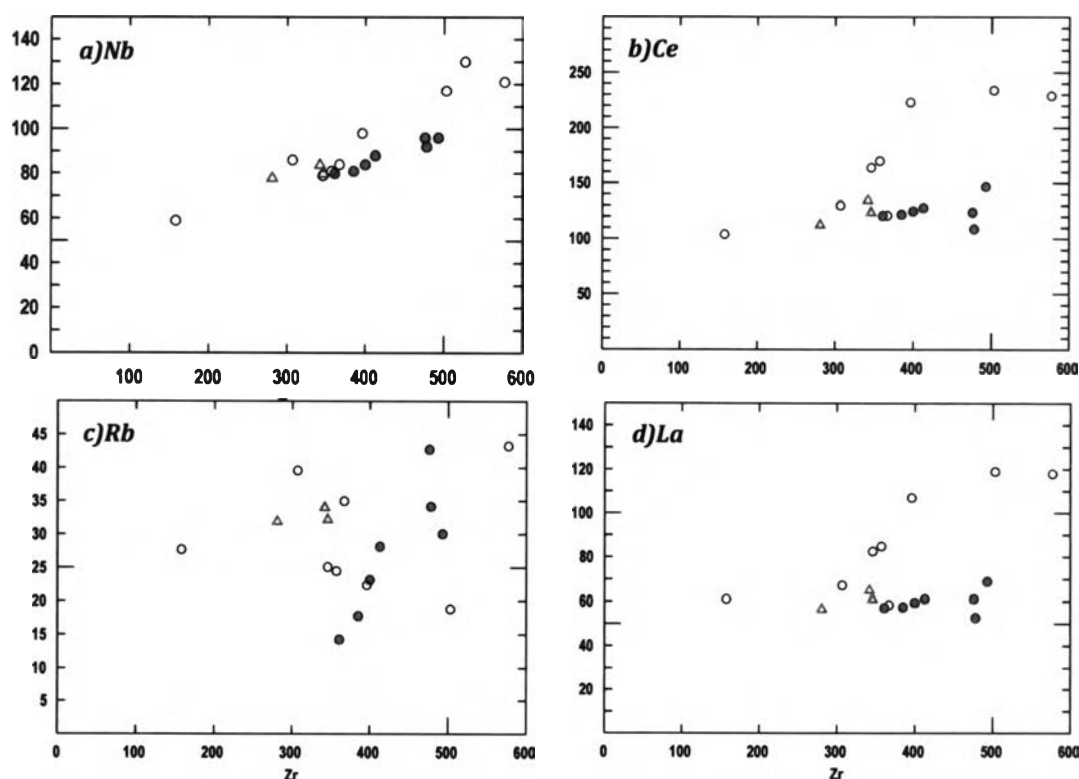

Figure 2.7 Plots of Nb, Rb, Ce and La versus Zr for basaltic rocks from the Nguu Huills, Ngulai Hils, and Kiboko (Chyulu) lavas. Symbols are the same as in Figure 2.5.

Based on pyrolite mantle-normalized multi-element diagrams (McDonough and Sun, 1995), the patterns are generally indifferent for all the basalt samples (Figures 2.8a-c). They all clearly exhibit negative anomalies of K and P. Slightly negative anomaly of U is also observed. A positive Nd anomaly is common; however, a slightly positive Ti spike is observed only in the Nguu specimens. This overall identical incompatible element patterns imply similarity in parental source material among the Nguu, Ngulai and Kiboko (Chyulu) basalts. Regardless of strong depletion of K, the overall patterns of these incompatible plots are quite similar to that of oceanic island basalts (OIB) suggesting a mantle plume-related process that induces partial melting in the upper mantle region. The strong depletion of K relative to other incompatibles further suggests an involvement of a K-bearing phase. There are 2 possible causes involved: (1) crystal fractionation of a K-bearing phase, e.g. amphibole and/or phlogophite, or (2) partial melting of a source which K-bearing phase has been retained in the source region. However, there is no amphibole or phlogophite phenocrysts observed. Therefore, the second possibility is the most plausible explanation for this effect. A slight spike of Ti in the Nguu basalts could be the effect of Ti-bearing mineral accumulation. This is supported by the presences of more abundant ilmenite and titanomagnetite observed in the Nguu rocks in forms of both phenocrysts and a matrix constituent compared to those found in the Kiboko and Ngulai basalts.

Based on chondrite-normalized REE spider diagrams (Sun and McDonough, 1989), all the studied basaltic samples have identical REE patterns (Figures 2.9a-c). They show the patterns of light REE enrichment relatve to heavy REE. No Eu anomalies observed on the patterns indicate no involvement of plagioclase fractionation for the lavas from the study areas.The steep negative slopes patterns further imply that these basalts have been derived from low degree partial melting of mantle and left either garnet or spinel behind.

The similarity of both normalized trace element and REE spider patterns (Figures 2.8 and 2.9) suggests that all the basalts from the Nguu, Ngulai and Kiboko areas may be generated from the same parental source or otherwise the souces share simimar chemical characteristics. This also implies that the mantle source underneath the area is quite homogeneous.
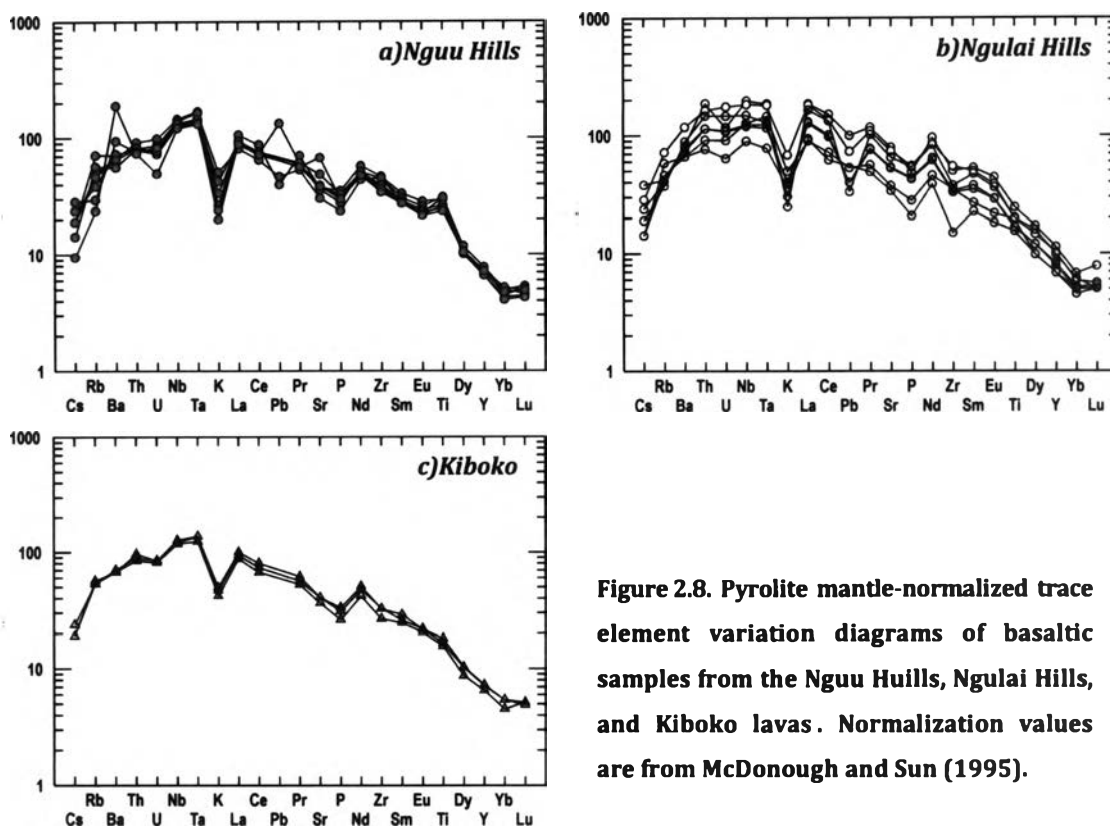
Figure 2.8. Pyrolite mantle-normalized trace element variation diagrams of basaltic samples from the Nguu Huills, Ngulai Hills, and Kiboko lavas. Normalization values are from McDonough and Sun (1995).
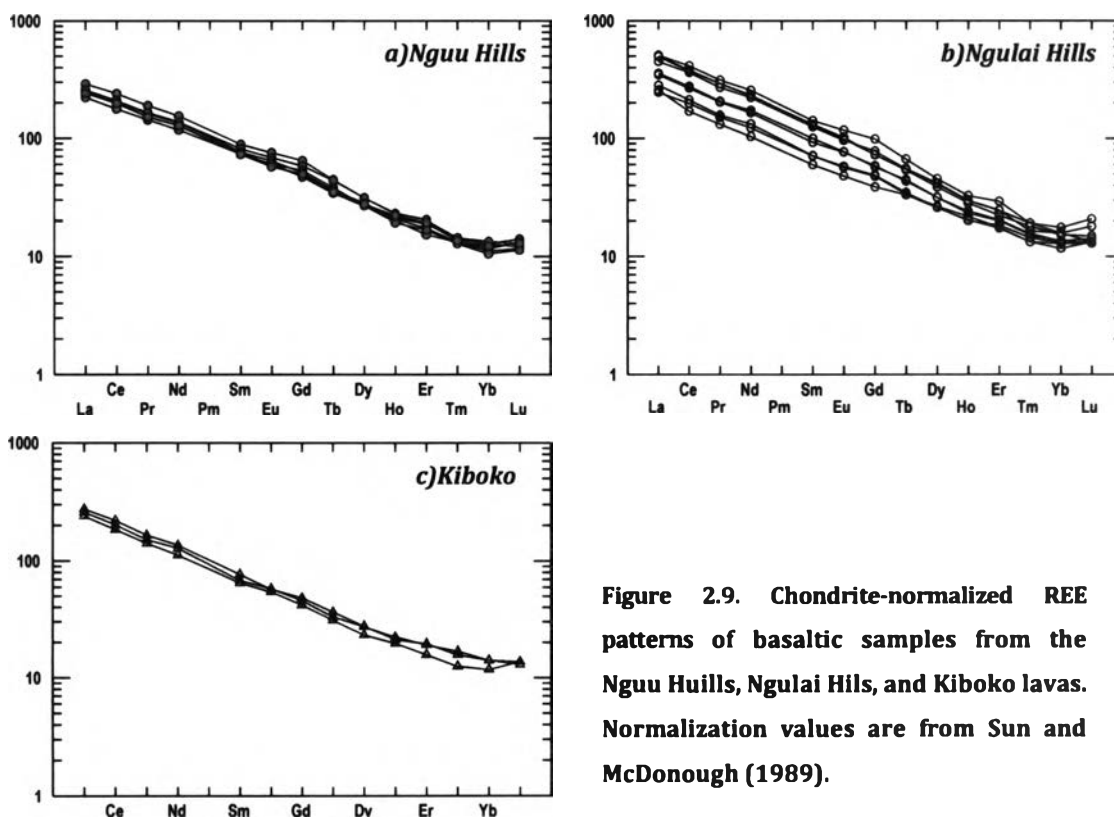

Figure 2.9. Chondrite-normalized REE patterns of basaltic samples from the Nguu Huills, Ngulai Hils, and Kiboko lavas. Normalization values are from Sun and McDonough (1989).

2.4 Geochronology

Seven basalt specimens were selected for ^{40}Ar/^{39}Ar dating in order to confine a time span for eruption events of these basalt units. Samples *KNg05, 06* and *08*, were chosen to represent the Nguu Hills basalts; whereas samples *KKNt 01* and *KKMb01* are for the Ngulai Hills basalts, and samples KKb01 and 02 are for the Kiboko (Chyulu) basalts. All specimens were incrementally heated from 550°C up to at either 1,400 or 1,500°C to ensure that all the argon gases released. However, at high temperature steps, above 1,000°C, all the specimens seem to be suffered from atmospheric contamination giving out unrealistic negative apparent ages at these steps affecting integrated, or so-called total-gas, ages obtained to be under estimated. Some data modifications are, therefore, needed to be made by discarding all those atmospheric contaminated steps and recalculating for integrated ages. The modified analytical data are listed in Table 2.6 and age spectrum diagrams of the samples are shown in Figure 2.10.

Results: The Ngulai sample, *KKNt01*, yields the oldest plateau age of 2.01±0.09 Ma estimated from 4 incrementally heating steps from 650-800°C which comprise 57% of 100% modified total ^{39}Ar released (Figure 2.10d). The Nguu basalts, on the other hand, are younger from 0.89 ± 0.07 (*KNg05a*) to 1.59 ± 0.13 (*KNg08a*) Ma. The plateau age of the *KNg08a* sample, which gives the oldest age for the Nguu lavas, was estimated based on 46% modified total gas released of 4 heating steps from 750-900°C (Figure 2.10a). The *KNg06a* sample with age of 1.13±0.03 Ma is obtained from 89% of the modified total gas released from 6 heating steps from 550-800°C, displays the best concordant release spectrums among all the analyzed specimens (Figure 2.10b). The *KNg05a* sample provides a plateau age of 0.89 ± 0.07 Ma according to 7 heating steps from 600-900°C with 93% modified total gas released (Figure 2.10c). The *KKb02* sample collected near Kiboko Spring gives out the youngest plateau age of 0.38±0.14 Ma, estimated from 3 heating steps from 1050-1150°C with about 63% of the modified total gas released (Figure 2.10e). Most specimens mentioned above have modified integrated ages consistent with the plateau ages, but the *KKb02* has an integrated age, 0.7±0.1 Ma, almost twice higher than the plateau age. This is caused by some instrumental Ar contamination during heating from 650, 700 and 800°C, as indicated by low atmospheric percentage values, which yield abnormal high dates of up to 2.5 Ma. The integrated age of KKb02 is

interpreted herein not represent the real-good age and not regarded as the geologically meaningful age.

Table 2.6 $^{40}Ar/^{39}Ar$ analytical data for dated specimens. Rows with bold italic numeric represent a set of heating step selected for plateau age estimation.

KKNt01a (304.0 mg)	J-value: 0.004190096 +/- 0.000002920						Air-shot_ratio: 291.042		
T(°C)	Cumulative 39Ar	Atmos. (%)	36Ar/ 39Ar	37Ar/ 39Ar	38Ar/ 39Ar	40Ar/ 39Ar	40Ar/ 36Ar	Age (Ma)	+/-
550	0.08	89.59	0.01	0.10	0.02	2.43	332.60	1.9	0.3
600	0.26	83.21	0.00	0.07	0.02	1.13	362.30	1.4	0.1
650	*0.45*	*89.53*	*0.01*	*0.05*	*0.02*	*2.73*	*333.00*	*2.1*	*0.2*
700	*0.61*	*91.44*	*0.01*	*0.06*	*0.02*	*2.84*	*325.90*	*1.8*	*0.1*
750	*0.73*	*91.43*	*0.01*	*0.07*	*0.02*	*3.07*	*325.60*	*2.0*	*0.2*
800	*0.83*	*91.95*	*0.01*	*0.08*	*0.02*	*3.50*	*323.40*	*2.1*	*0.3*
850	0.90	95.37	0.01	0.12	0.02	4.11	311.30	1.4	0.1
900	0.96	95.78	0.02	0.17	0.02	4.92	309.50	1.6	0.3
950	1.00	99.70	0.02	0.35	0.03	6.34	296.50	0.1	0.3

Plateau Age = 2.01 +/- 0.09 Ma
(4 steps: 57% fract^n ^{39}Ar) MSWD = 0.98
Integrated Age = 1.7 +/- 0.1 Ma
39Ar volume = 0.1354E-09 ccSTP/g

Isochron age = 0.39 +/- 0.58 Ma
MSWD = 0.7143
Reciprocal of Y-intercept = 300.19 +/- 3.20
40Ar* volume = 0.1680E-10 ccSTP/g

KNg08a (254.0 mg)	J-value: 0.004190096 +/- 0.000002920						Air-shot_ratio: 290.991		
T(°C)	Cumulative 39Ar	Atmos. (%)	36Ar/ 39Ar	37Ar/ 39Ar	38Ar/ 39Ar	40Ar/ 39Ar	40Ar/ 36Ar	Age (Ma)	+/-
550	0.06	96.44	0.03	0.15	0.04	9.35	306.90	2.5	0.8
600	0.19	94.28	0.01	0.10	0.04	3.31	315.40	1.4	0.2
650	0.34	94.53	0.02	0.08	0.03	5.83	313.80	2.4	0.3
700	0.47	94.20	0.02	0.07	0.03	4.73	315.20	2.1	0.3
750	*0.60*	*94.81*	*0.01*	*0.06*	*0.03*	*4.33*	*313.40*	*1.7*	*0.3*
800	*0.72*	*94.45*	*0.01*	*0.05*	*0.02*	*3.92*	*314.90*	*1.6*	*0.2*
850	*0.84*	*95.46*	*0.01*	*0.04*	*0.02*	*4.25*	*311.40*	*1.5*	*0.3*
900	*0.93*	*96.16*	*0.02*	*0.06*	*0.02*	*5.41*	*308.70*	*1.6*	*0.2*
950	1.00	95.35	0.02	0.13	0.02	6.70	310.80	2.4	0.5

Plateau Age = 1.59 +/- 0.13 Ma
(4 steps: 46% fract^n ^{39}Ar) MSWD = 0.14
Integrated Age = 1.9 +/- 0.1 Ma
39Ar volume = 0.9667E-10 ccSTP/g

Isochron age = 1.69 +/- 0.21 Ma
MSWD = 0.4413
Reciprocal of Y-intercept = 294.54 +/- 6.61
40Ar* volume = 0.2375E-10 ccSTP/g

Table 2.6   (cont.)

KNg06a (296.0 mg)		J-value: 0.004190096 +/- 0.000002920						Air-shot_ratio: 291.274	
T(°C)	Cumulative 39Ar	Atmos. (%)	36Ar/ 39Ar	37Ar/ 39Ar	38Ar/ 39Ar	40Ar/ 39Ar	40Ar/ 36Ar	Age (Ma)	+/-
550	*0.11*	*95.38*	*0.01*	*0.02*	*0.02*	*3.03*	*312.60*	*1.1*	*0.1*
600	*0.34*	*89.66*	*0.00*	*0.02*	*0.02*	*1.44*	*336.00*	*1.1*	*0.1*
650	*0.55*	*93.60*	*0.01*	*0.02*	*0.02*	*2.28*	*319.50*	*1.1*	*0.1*
700	*0.71*	*92.89*	*0.01*	*0.02*	*0.02*	*2.16*	*322.10*	*1.1*	*0.1*
750	*0.82*	*91.79*	*0.01*	*0.03*	*0.02*	*2.15*	*325.90*	*1.3*	*0.1*
800	*0.89*	*93.56*	*0.01*	*0.03*	*0.02*	*2.31*	*319.40*	*1.1*	*0.1*
850	0.95	97.30	0.01	0.05	0.02	2.57	306.70	0.5	0.3
900	1.00	97.36	0.01	0.09	0.02	3.33	305.50	0.7	0.3

Plateau Age =1.13 +/- 0.03 Ma   Isochron age = 1.16 +/- 0.23 Ma
(6 steps: 89% fractⁿ 39Ar) MSWD = 1.43   MSWD = 1.33
Integrated Age = 1.1 +/- 0.0 Ma   Reciprocal of Y-intercept = 294.90 +/- 3.02
39Ar volume = 0.3674E-09 ccSTP/g   40Ar* volume = 0.1459E-10 ccSTP/g

KNg05a (298.0 mg)		J-value: 0.004190096 +/- 0.000002920						Air-shot_ratio: 290.688	
T(°C)	Cumulative Fractⁿ 39Ar	Atmos. (%)	36Ar /39Ar	37Ar /39Ar	38Ar /39Ar	40Ar /39Ar	40Ar /36Ar	Age (Ma)	+/-
600	*0.13*	*96.66*	*0.01*	*0.05*	*0.03*	*4.22*	*307.50*	*1.1*	*0.2*
650	*0.29*	*97.53*	*0.02*	*0.07*	*0.03*	*6.01*	*304.20*	*1.1*	*0.1*
700	*0.46*	*97.87*	*0.02*	*0.07*	*0.02*	*4.66*	*303.50*	*0.7*	*0.2*
750	*0.60*	*96.99*	*0.01*	*0.07*	*0.02*	*3.90*	*306.50*	*0.9*	*0.2*
800	*0.73*	*97.58*	*0.01*	*0.06*	*0.02*	*3.43*	*305.00*	*0.6*	*0.3*
850	*0.84*	*96.98*	*0.01*	*0.08*	*0.02*	*3.80*	*306.50*	*0.9*	*0.2*
900	*0.93*	*97.64*	*0.02*	*0.09*	*0.02*	*4.89*	*304.00*	*0.9*	*0.2*
950	1.00	99.32	0.02	0.13	0.02	5.86	298.50	0.3	0.3

Plateau Age =0.89 +/- 0.07 Ma   Isochron age = 0.39 +/- 0.58 Ma
(7 steps: 93% fractⁿ 39Ar) MSWD =0.86   MSWD = 0.71
Integrated Age = 0.8 +/- 0.1 Ma   Reciprocal of Y-intercept =300.19 +/- 3.20
39Ar volume = 0.1509E-09 ccSTP/g   40Ar* volume = 0.1680E-10 ccSTP/g

KKb02 (207.0 mg)		J-value: 0.004319107 +/- 0.000005036						Air-shot_ratio: 304.667	
T(°C)	Cumulative Fractⁿ 39Ar	Atmos. (%)	36Ar /39Ar	37Ar /39Ar	38Ar /39Ar	40Ar /39Ar	40Ar /36Ar	Age (Ma)	+/-
650	0.05	75.11	0.00	0.48	0.02	0.80	384.00	1.5	1.0
700	0.14	72.34	0.00	0.45	0.02	0.81	399.50	1.7	0.5
750	0.23	99.12	0.00	0.49	0.02	0.72	294.60	0.1	0.4
800	0.31	52.70	0.00	0.54	0.02	0.69	524.40	2.5	0.5
1050	*0.54*	*82.11*	*0.00*	*1.49*	*0.02*	*0.47*	*292.80*	*0.6*	*0.1*
1100	*0.81*	*91.58*	*0.00*	*6.02*	*0.01*	*0.57*	*177.90*	*0.4*	*0.3*
1150	*0.94*	*99.82*	*0.00*	*8.27*	*0.02*	*0.76*	*165.80*	*0.01*	*0.2*
1200	1.00	89.13	0.01	10.99	0.01	1.27	193.90	1.1	0.5

Plateau Age =0.38 +/- 0.14 Ma   Isochron age = -0.47 +/- 0.10Ma
(3 steps: 63% fractⁿ 39Ar) MSWD =3.6   MSWD = 0.65
Integrated Age = 0.7 +/- 0.1 Ma   Reciprocal of Y-intercept =301.78 +/- 15.82
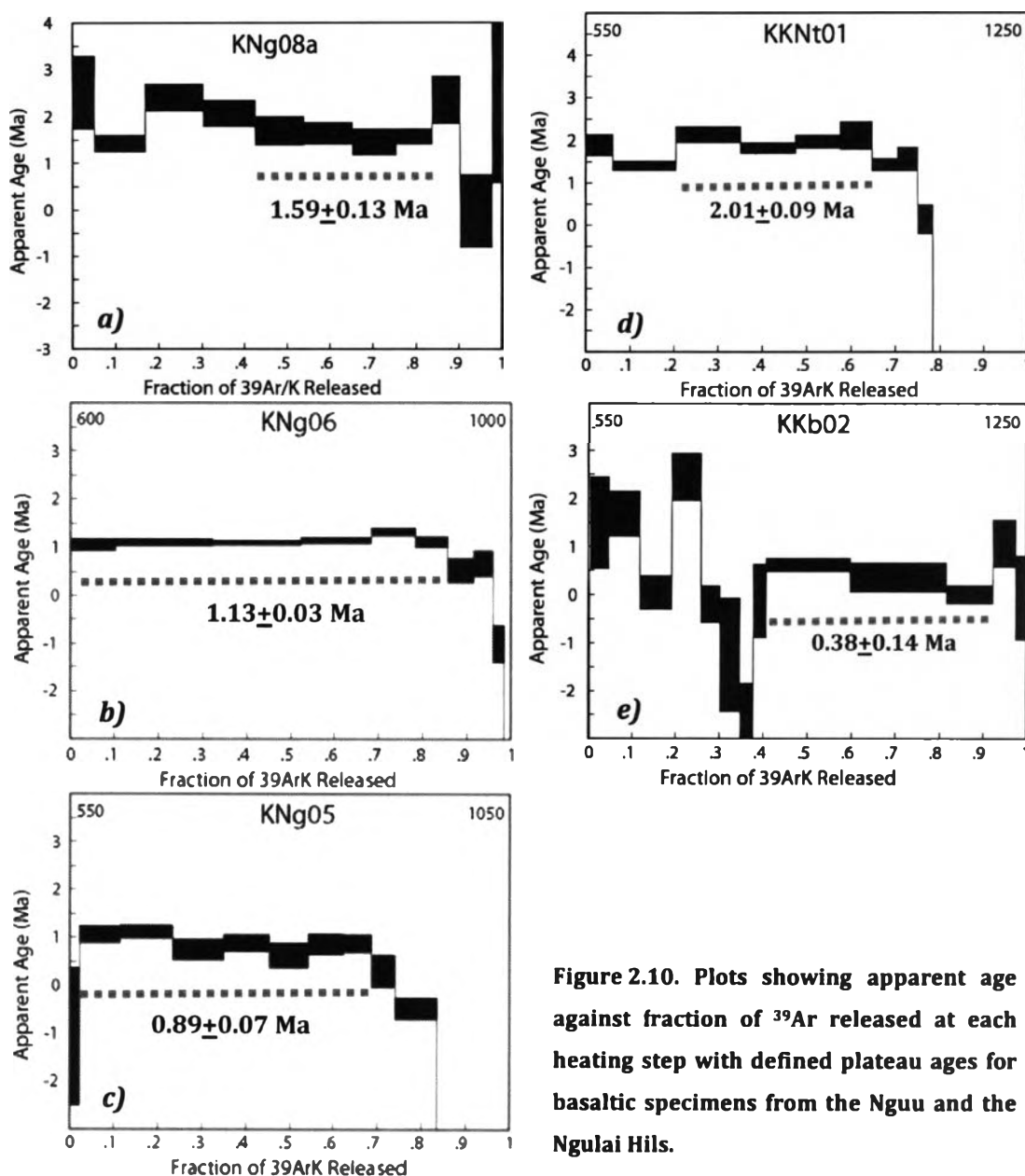39Ar volume = 0.1735E-09 ccSTP/g   40Ar* volume = 0.1635E-10 ccSTP/g

Figure 2.10. Plots showing apparent age against fraction of ³⁹Ar released at each heating step with defined plateau ages for basaltic specimens from the Nguu and the Ngulai Hils.

There are two specimens, *KKMb01a* and *KKb01a*, which do not provide any meaningful age. The *KKMb01a* sample has a nice negative plateau age (-0.21±0.09 Ma; Figure 2.11a). This might suggest that the age of the specimen is affected by atmospheric contamination or it is too young to be detected. The *KKb01a* sample, on other hand, seems to displays two plateau ages of 1.28±0.13 and 0.47±0.12 Ma (Figure 2.11b). This might imply that 1.28±0.13 Ma could represent an actual age of the rock, which is responding to the Nguu basalts exposed nearby, whereas 0.47±0.12 Ma might suggest a later overprint event caused by a younger volcanic activity of

samples, particularly for *KKb01*, might not be valid since the fractions of $^{39}Ar/K$ released for each plateau age estimated are about 20% and 30% respectively which is generally too small to be considered significant. Therefore, repeating analyses on these specimens are necessary to ensure this interpretation.
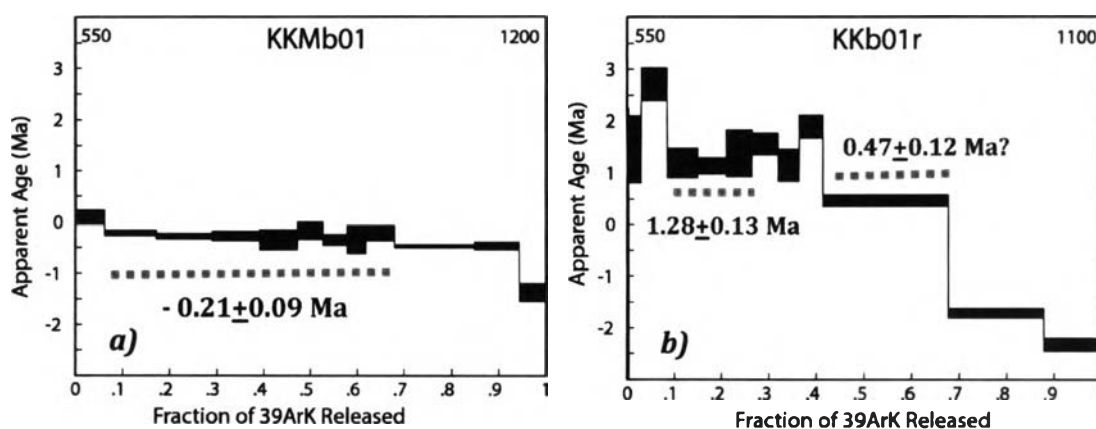

Figure 2.11. Plots showing apparent age against fraction of ^{39}Ar released at each heating step for selected basaltic specimens from the Ngulai Hils and the Chyulu (Kiboko) lavas of which meaningful plateau ages cannot be clearly defined.

When combining with LeBas *et al.* (1986) classification diagram, this sample suite clearly exhibits Ar-Ar age decreasing trend toward the more fractionated end (Figure 2.12). The *KKNt01a* sample which are among the studied basalts with the most primitive composition yields the oldest age while the *KKb02* sample which compositionally falls in the most fractionated region has the youngest age. The samples *KNg08a, 06a,* and *05a* with intermediate age range also fit well in the middle part of the fractionation trends. This indicates that the basaltic volcanism within the study area had intermittently occurred several times during late Pliocene to middle Pleistocene. As magma compositions became more felsic and more silica saturate through times, this may suggest that partial melting generated batches of magma which may have been stagnating above the source region that periodically ejected a portion of the melts to the surface and left the rest at depth to experience further crystal fractionation process while waiting for the next round of eruption. This interpretation is also supported by petrographic features observed, e.g. coarser groundmass and more modal percentages of clinopyroxene and plagioclase
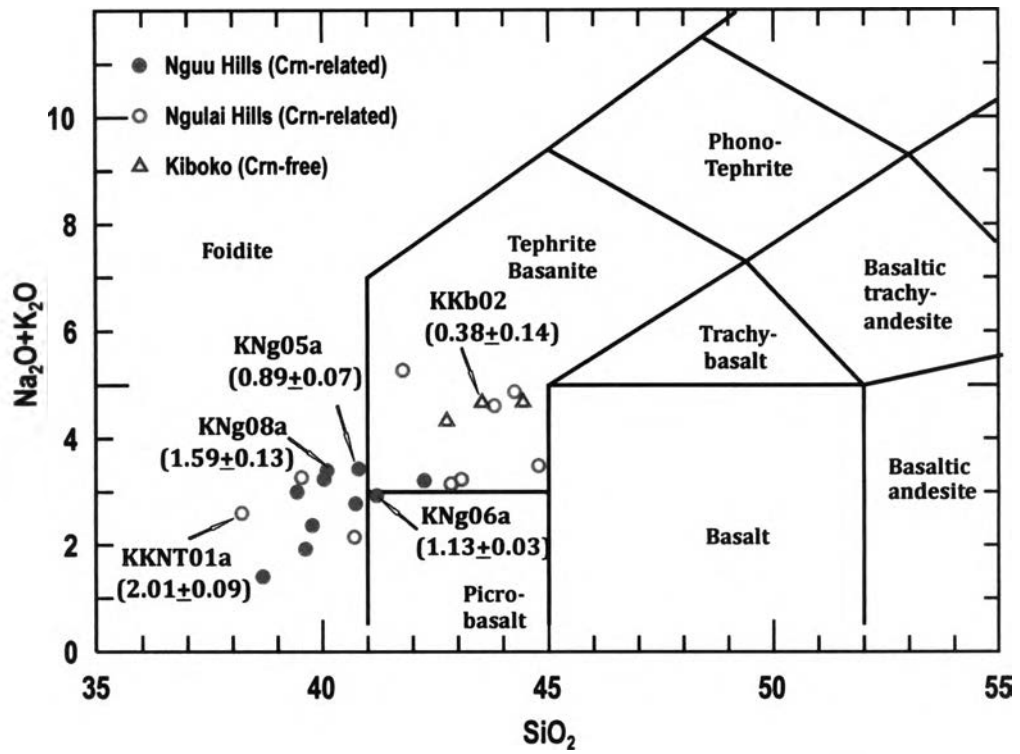
Figure 2.12. Plots showing plateau age of the dated specimen along the fractionation trends of the basalts from the study area.